

Original Research

Investigation on Properties and Heavy Metal Ion Extraction of Thermally Activated Red Mud Incorporated Cement Mortar

K. Athira, T. Shanmugapriya*

School of Civil Engineering, VIT, Vellore, Tamil Nadu, India

Received: 1 January 2023

Accepted: 22 March 2023

Abstract

This study introduced the red mud as a filter of heavy metal ions in cement mortar by partial cement replacement. The raw red mud and thermally activated red mud at three different temperatures, 650, 700, and 750°C represented as RM650, RM700, and RM750 were comprehensively analyzed to find an optimum processing temperature as a better cement replacement for metal extraction. The Atomic Adsorption Spectroscopic (AAS) process evaluated the metal extraction capacity of raw and thermally treated red mud from their respective standard solutions. The optimum processing temperature of red mud was decided by Thermogravimetric analysis (TGA), X-ray fluorescence spectroscopy (XRF), X-ray diffraction (XRD), Fourier transform infrared (FTIR), and Field emission scanning electron microscope (FE-SEM), and pozzolanic activity. Test results show that the temperature stimulates the formation of CaO, Al₂O₃, and Fe₂O₃, which decides the pozzolanic activity of the material. Red mud calcined at 700°C (RM700) was found as an optimum calcination temperature with reactive, crystalline compounds. RM700 showed the maximum pozzolanic activity and better heavy metal ion extraction capacity. The extraction ability of all red mud samples was in the sequence of Cr>Cd>Pb>Cu. The experimental results of metal extraction capacity and the pozzolanic activity were analyzed and validated by establishing linear regression models to predict a statistically significant mathematical model.

Keywords: red mud, microstructural characterization, calcination, metal extraction

Introduction

The manufacturing process of aluminum results in a toxic and highly alkaline by-product, red mud. The chemical composition of red mud varies based on the applied conditions during the production of

aluminum. However, hematite (α -Fe₂O₃), goethite (α -FeOOH), boehmite (γ -AlO(OH)), and quartz (SiO₂) are the major compounds and calcite (CaCO₃) and gibbsite (Al(OH)₃) are the minor compounds that constitute in the raw red mud. The characteristic studies conclude that red mud reacting with water molecules releases OH⁻ ions contributing to high pH. With suitable treatment methods, red mud can be converted into cementitious material and used in the construction industry [1]. As per the studies, red mud calcined

*e-mail: shanmugapriya.t@vit.ac.in

at 550-900°C temperatures shows better pozzolanic activity [2, 3]. However, when considering calcined red mud, CO₂ emission is more prominent. Calcination above 750°C possesses decarbonation of calcite to quick lime and CO₂ [4-6]. Thus, it would adversely affect the Global Warming Potential, Cumulative Energy Demand, and the emission of major air pollutants (CO, NO_x, PM₁₀, and SO₂) adversely [7]. Therefore, the calcination temperature must be maintained to acquire a lower environmental burden while replacing cement with calcined red mud. Red mud develops amorphous C-S-H gel of lower Ca/Si ratio with higher surface area and large pore volume. Because of the highly alkaline nature of the red mud, the total alkalinity of the activator would increase. Moreover, it would support the dissolution of aluminosilicate material and the condensation of aluminosilicate gel, eventually resulting in the rise of the ratio of Na₂O/SiO₂ in the mix [8].

Red mud is a promising economical photocatalyst used in cement composites with other chemical compounds, such as Niobium pentoxide (Nb₂O₅), to produce the self-cleaning surface [9]. Higher specific surface area, optical absorption, and photocurrent response of calcined or modified red mud were utilized to remove organic and inorganic pollutants from the aqueous solutions [10]. Due to its high specific surface area, red mud has several adsorption sites; hydroxides of aluminum and iron mineral phase, gibbsite, and hematite. Calcined red mud, combined with graphitic carbon nitride (CN), reacts to form RM-CN composite photocatalyst and is used to remove pollutants like dye and antibiotics from wastewater [10]. The calcination process improves the dispersion of red mud particles in the aqueous solution and promotes the effective degradation of heavy metals. The two different studies conducted by Shi et al. (2020) [11, 12] explain the reason for the photocatalytic effect of red mud, possibly due to calcite (CaCO₃), cancrinite [Na₈(Al₆Si₆O₂₄)(OH)_{2,04}(H₂O)_{2,66}], anatase (TiO₂), hematite (α-Fe₂O₃) and tridymite (SiO₂) in red mud as that of carbon nitride (CN), titanium dioxide (TiO₂), and ferric oxide (Fe₂O₃).

In a recent study conducted by Oprčkal et al. (2020), Red Mud (RM) was used to immobilize the Potentially Toxic Elements (PTEs) presented in the Contaminated Soil (CS). The mechanism of adsorption of PTEs of CS/RM composition was well explained as the sorption and precipitation process. The adsorption was relatively faster except Cd, Pb, and Zn, as most of the immobilization processes presented in this study were found to be independent of time [13]. However, Cd, Pb, and Zn had a time-dependent immobilization rate, probably due to the slow diffusion of ions [12, 13]. In another study, Chen et al. (2019) investigated the enhanced extraction efficiency of red mud Ground Glass Granulated Blast Furnace Slag (GBFS) pervious geopolymer concrete over ordinary Portland cement pervious concrete due to the high surface reactive particles in the micron and sub-micron size range present in the red mud. After 50 purification cycles,

the extraction capacity of red mud GBFS pervious geopolymer concrete was 18.4, 17.91, 25.07, and 39.18% for Cd²⁺, Pb²⁺, Cu²⁺, and Cr³⁺, respectively [14].

The vast range of red mud in the applications such as photocatalytic effect and metal extraction can collaborate with the construction industry as a Supplementary Cementitious Material (SCM). So far, red mud, along with other chemicals, are combined to achieve the photocatalytic effect and metal extraction properties. In cement composites, introducing other chemicals may lead to complex reactions and adversely affect the actual purpose. Therefore, in this study, the influence of thermal activation of red mud in metal extraction property concerning pozzolanic activity is analyzed through extensive chemical and microstructural studies. An optimum calcination temperature is proposed to obtain a satisfactory strength activity index. The effect of metal extraction capacity on raw and calcined red mud has been investigated and is statistically analyzed using a linear regression model and ANOVA (Analysis of Variance) techniques.

Materials

The binder materials used were cement, raw red mud, and calcined red mud. Raw and calcined red mud was tested on specific properties like metal extraction for further application-based studies. In this investigation, red mud is collected from HINDALCO, Belgaum. The cement of grade 53 with a specific gravity of 3.15 and river sand with a specific gravity of 2.67 is used. The red mud collected from the site was oven dried for 24 h at 105°C and crushed until it passed through a 150 μm sieve. Powdered red mud was calcined in an electrical tilting furnace at 650, 700, and 750°C for 3 h. The percentage by mass of compounds present in cement and red mud is given in Table 1. Cement contains a high percentage of lime and silica and a low amount of alumina and iron oxide compared to red mud.

From Table 1, red mud is rich in Al₂O₃ and Fe₂O₃; poor in SiO₂ and CaO content compared to cement. The temperature enhanced the percentage of SiO₂ and Al₂O₃. However, Fe₂O₃ content has dropped down as the temperature increased. CaO content increased slightly until 700°C calcination compared to raw red mud and decreased at 750°C, agrees with the study conducted by Karunadasa et al. (2019). However, beyond 700°C, CaO percentage is decreased by percentage composition due to the decomposition process of CaO at higher temperature [15].

Experimental Methods

Thermogravimetric Analysis (TGA)

The quantitative changes of raw red mud at high temperatures were studied by Thermogravimetric

Table 1. Chemical composition of cement and red mud.

Compounds	Cement	Red mud			
		Raw	650°C	700°C	750°C
SiO ₂	19.70%	10.00%	10.20%	10.31%	11.31%
TiO ₂	0.45%	6.08%	5.93%	6.09%	7.43%
Al ₂ O ₃	4.83%	22.50%	22.51%	23.20%	23.51%
MnO	6 ppm	6 ppm	701 ppm	725 ppm	882 ppm
Fe ₂ O ₃	4.71%	44.30%	44.30%	43.10%	40.51%
CaO	65.70%	5.82%	6.25%	6.35%	3.94%
MgO	0.97%	0.54%	0.65%	0.55%	0.47%
Na ₂ O	0.22%	8.54%	7.53%	8.92%	10.81%
K ₂ O	0.45%	0.12%	0.11%	0.13%	0.20%
P ₂ O ₅	0.29%	0.30%	0.28%	0.34%	0.35%

analysis and carried out using SDT Q600 - TA instruments at a controlled temperature. Step-by-step chemical changes occurred in raw red mud for a gradual rise in temperature from 0 to 800°C can be obtained.

Calcination Process

The three steps performed in processing red mud are oven drying, crushing, and calcination (Fig. 1). The raw red mud collected from the plant was oven dried for 24 h to remove the water molecules in the external pores. Dried red mud was crushed and made into a fine powder that can pass through a sieve of size 45 μm. Fine red mud underwent calcination at high temperatures in a stir-casting furnace of 5 kg for 3 h. The minimum time required to decompose the compounds to attain pozzolanic activity is 3 h [16].

X-Ray Fluorescence Spectroscopy (XRF)

The chemical compositions of cement and raw and calcined red mud were obtained and analyzed from the XRF results. The quantitative elemental determination was done with Bruker model S8 Tiger and S4 Pioneer sequential wavelength-dispersive X-ray spectrometers. 4 kW Rh X-ray tube was used to produce X-rays, and SPECTRAplus software was used for further analysis.

X-Ray Diffraction (XRD)

The crystalline characteristics of material samples are analyzed by X-ray diffraction was done. By revealing the crystalline phase, the chemical composition of the materials has also been revealed. The X-ray powder diffraction pattern was collected on a Bruker

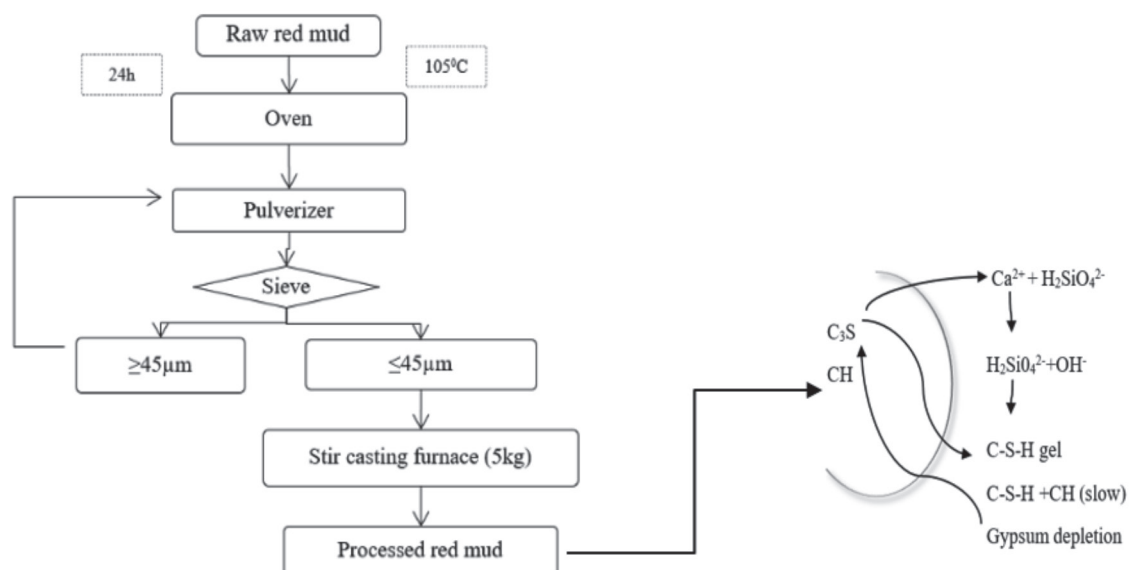


Fig. 1. Process of thermal activation of red mud.

diffractometer (D8 Advance model, Germany) with theta/2theta geometry source operating a ceramic tube at 2.2 kW and a copper anode. The detector is equipped with a Lynx eye detector working under silicon strip detector technology. The X-ray diffraction pattern was recorded in the 10° - 70° 2θ range with a step size of 0.014° for all specimens. The counting time was recorded as 23 s per step.

Fourier Transform Infrared Spectroscopy (FTIR)

FTIR of raw and calcined red mud was performed to analyze the phase formed due to the thermal activation of red mud. IR affinity 1, Shimadzu FT-IR Spectrophotometer is used. The equipment has a resolution of 0.5 - 16 cm^{-1} and a 4000 - 400 cm^{-1} spectral range. The functional group is observed in the established absorption band and detects the formations of various compounds at different calcination temperatures.

Field Emission Scanning Electron Microscopy (FESEM)

The surface morphology of the samples was analyzed with Thermo Fisher FEI QUANTA 250 FEG with a 5 kV to 20 kV operating voltage range. The samples' micromorphological images with a high resolution of 1.2 nm at high voltages under high vacuum conditions were obtained. The compositional analysis of raw and calcined red mud was availed from the FESEM analysis combined with EDS. Since the samples are non-conducting, the gold coating has been done to get a non-reflective micrograph.

Pozzolanic Activity

The strength activity index value has been used for investigating the suitability of the processed red mud for cement replacement. As per ASTM C311/311M [16], 20% cement in the control mixture was replaced by red mud calcined at different temperatures to prepare three batches of specimens. Six samples were cast for each batch for testing 7 and 28 days of compressive strength. The control mixture consists of 500 g of Portland cement, 1375 g of graded standard sand and

242 mL of water. The mortar mixes represented as P0, P1, P2, P3, and P4. P0 is the reference mix without any cement replacement by red mud, P1 is the mortar mix with cement replacement by oven dried red mud, P2 by RM650, P3 by RM700, and P4 by RM750. The mix design is given in Table 2.

Demoulded samples were cured in saturated lime water. The compressive strength of test specimens was determined and compared to the compressive strength of the reference specimens. The strength activity index was calculated for each red mud test specimen using the following formula.

$$\text{Strength activity index with Portland cement} = (A/B) \times 100 \quad (a)$$

Where:

A = average compressive strength of test mixture cubes, MPa, and

B = average compressive strength of control mix cubes, MPa.

Atomic Absorption Spectroscopy (AAS)

The instrument for AAS places the sample in a high flame fuelled by either nitrous oxide or acetylene. The flame provides atomic species and passes selected, illumination through the flame to detect what wavelengths of light the sample atoms absorb, and element specific. The red mud samples were dissolved in H_2SO_4 [17] and the standard solutions of heavy metals were prepared with a concentration of 1000 ppm. Potassium dichromate ($\text{K}_2\text{Cr}_2\text{O}_7$), lead chloride (PbCl_2), cadmium chloride (CdCl_2), and copper sulfate (CuSO_4) were examined with AAS to obtain the percentage of metal extraction by each sample. The acid taken is 99% pure sulphuric acid to dissolve the raw and calcined red mud samples [18, 19]. Standard solutions of heavy metal ions were considered for the metal extraction property of red mud samples. Notably, the time of contact with the red mud samples with heavy metal ions also influences the adsorption spectra significantly. In this study, a uniform contact time is considered in all the samples with each heavy metal ion.

Table 2. Mix design for the pozzolanic activity test of calcined red mud.

Sl. No.	Mix designation	Cement (gm)	Red mud (gm)	Sand (gm)	Water (mL)	No. of cubes	Remarks
1	P0	500	-	1375	272	6	Control
2	P1	400	100	1375	272	6	Raw red mud
3	P2	400	100	1375	272	6	650°C
4	P3	400	100	1375	272	6	700°C
5	P4	400	100	1375	272	6	750°C

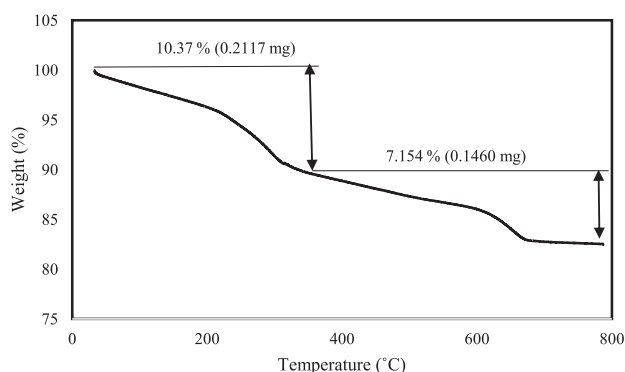


Fig. 2. TGA results of red mud.

Results and Discussions

Thermogravimetric Analysis (TGA)

In Fig. 2, at 250-300°C may be due to water loss from internal pores and channels and the escape of water from hydrated compounds like silicate, sulfate, and aluminate. Other events recorded at 300-500°C explain the decomposition of gibbsite $\{Al(OH)_3\}$ or the formation of aluminium oxide due to the dehydration of boehmite. Over 600°C due to pyrolysis, $Al(OH)_3$ changes its chemical composition. The presence of tricalcium silicate or hatrurite and gehlenite ($Ca_2Al_2SiO_7$) was identified between 800 and 900°C. Which is identified and explained in XRD (Fig. 4). Further calcination will not cause any change in the chemical composition of certain constituents like dicalcium silicate (Ca_2SiO_4), hematite (Fe_2O_3), perovskite ($CaTiO_3$), and CaO [20]. Generally, the weight loss is up to 27-29% till the 500°C rise and 5-6% from 500-800°C temperature rise [21] (Fig. 2). Above 900°C, no considerable mass change has been observed [20]. Table 3 gives decomposition steps at different temperatures during the thermal treatment conducted. The decomposition results obtained in this study agree well with the previous studies conducted by various authors and are given in Table 3.

Over 600°C, the red mud starts to improve its pozzolanic activity due to the formation of silica and

alumina compounds (Table 1), which is in agreement with the previous studies [24-26]. However, calcination beyond 700°C causes decarbonation of calcite (calcium carbonate), and quick lime formation happens, adversely affecting the reactivity. Pera et al. (1997) suggested pre-hydrating calcined red mud with 25% water before mixing to form a cement composite to overcome the less reactivity possessed by red mud calcined at a temperature above 700°C [24]. The reaction of water with quick lime leads to the formation of calcium hydroxide, resulting in a faster hydration process and better binding properties in cement composites. Here, despite such techniques, only the pozzolanic activity measurement of red mud samples due to thermal activation is considered. Therefore, considering the primary pozzolanic compound formation (Table 3), the temperatures chosen are 650, 700, and 750°C for further studies.

X-Ray Diffraction (XRD)

The X-ray diffractograms of oven-dried and calcined red mud at 650, 700, and 750°C are shown in Fig. 3. The XRD data of red mud at different temperatures gave a non-uniform chemical composition pattern. As the temperature increased, the peaks represented gibbsite and boehmite vanished. However, goethite ($FeO(OH)$), hematite ($\alpha-Fe_2O_3$) (which at higher temperatures changes to magnetite), and calcite formed a dominant phase since they are retained throughout, irrespective of the temperature rise. Here, red mud calcined at a different temperature exhibited a weak, moderate, and highly alkaline nature. The oxides of calcium and sodium contribute to the alkalinity of red mud. The temperature increment reduces the decarbonation process in red mud. The oven-dried sample over 100°C contained a weak OH group and disappeared when the temperature increased to 650°C. At low temperatures, the compounds are amorphous; as the temperature exceeds 750°C, the crystallinity increases. The crystallization process changes the microstructure and reduces the alkalinity of red mud effectively. The variation in alkalinity of red mud samples was

Table 3. Chemical changes of red mud due to temperature increase.

Temperature °C	Chemical Change	% Weight Loss	Reference
60-100	Removal of adsorbed water	10.66	[22]
200-500	$Al(OH)_3 \rightarrow AlO(OH)(s) + H_2O(g)$ (Gibbsite to boehmite) $AlO(OH)(s) \rightarrow Al_2O_3 + H_2O(g)$ (Boehmite to alumina)	17.00	[22, 23]
550-800	$CaCO_3 \rightarrow CaO + CO_2$ (Decomposition of calcite) $3Fe_2O_3 \rightarrow 2Fe_3O_4 + 0.5O_2$ (Hematite to magnetite)	5.16	[20, 22, 23]

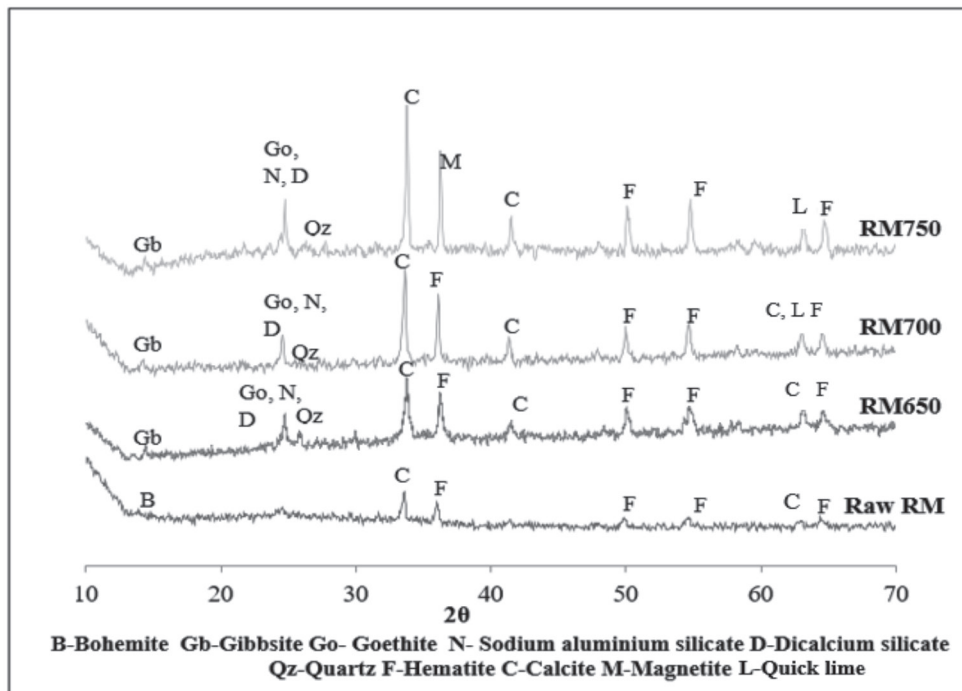


Fig. 3. XRD of raw and calcined red mud.

identified by measuring the pH of the raw and calcined red mud samples (pH of raw red mud, RM650, RM700, and RM750 are 13.06, 9.06, 8.07, and 8.01, respectively). The solid basic character dropped due to the decomposition of metal oxides to form poor or non-basic oxides. As the temperature exceeds 700°C, highly crystallized calcite, goethite, and magnetite are formed. Also, above 700°C, calcite decarbonation occurs and forms quick lime and CO_2 . The enhanced CO_2 emission due to decarbonation of calcite beyond 700°C adversely affects the development of a sustainable product.

Fourier Transform Infrared Spectroscopy (FTIR)

FTIR spectra show that the chemical composition of red mud is significantly affected by temperature (Fig. 4). Red mud comprises S-A-O and Al-A-O phases, which present unrepeated extending vibrations. It is evident from FTIR spectra that the vibrations are overlapping from the raw red mud to red mud calcined at 750°C. The peaks at a higher frequency are found to be the combinations of Al-A-O-S, S-A-OH, Al-A-OH, and S-A-OA-S vibrations. From 700°C, a small

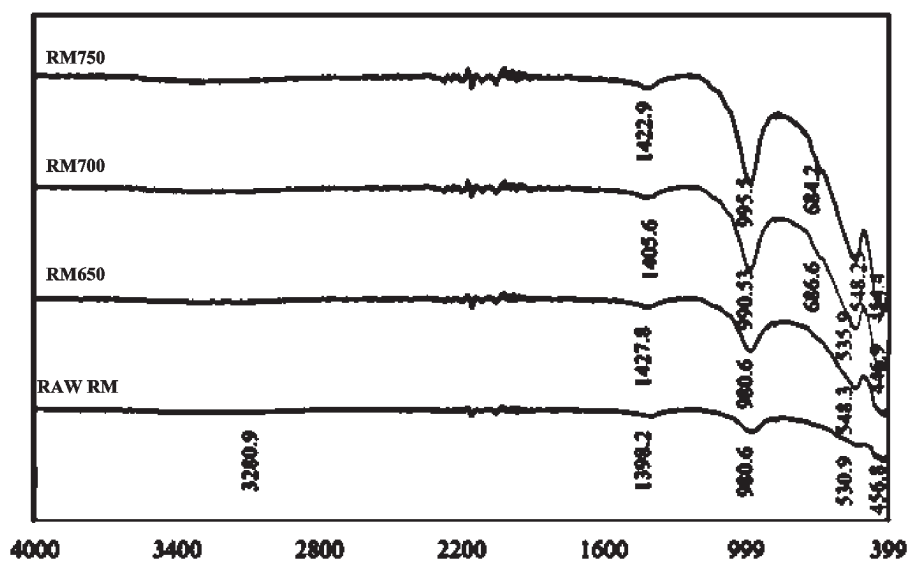


Fig. 4. FTIR spectra for raw red mud and red mud calcined at different temperatures.

peak at 670 cm^{-1} shows the formation of Tobermorite. A mild frequency band could be observed at 3280.9 cm^{-1} in raw red mud. It can be explained as the hydroxyl-stretching region and H_2O present in red mud [27]. This band disappeared as the temperature increased and was not present in the other samples of red mud. The $1400\text{--}1500\text{ cm}^{-1}$ bands ensure traces of CaO and S-O. Anti-symmetric vibrations similar to calcite were also observed, as explained by Borrajo et al. (2004) in their study [28]. The vibrations present in IR spectra from 450 cm^{-1} to 1000 cm^{-1} , such as in plane S-O bending, S-O stretching, and inside S-O tetrahedra vibrations, show the presence of quartz in red mud.

However, it is evident that, as the temperature rises, the band from 980.6 moves to higher frequencies due to the ongoing decomposition and breakage of bonds to form other compounds. Below 475 cm^{-1} , stretching vibration of the Fe-O bond was found.

FE-SEM and EDS

The micromorphological graph obtained from FE-SEM analysis of raw red mud and red mud calcined at 650 , 700 , and 750°C is given in Fig. 6. The water from external pores evaporates during the oven drying process. Therefore, in Fig. 6a), loosely packed red mud

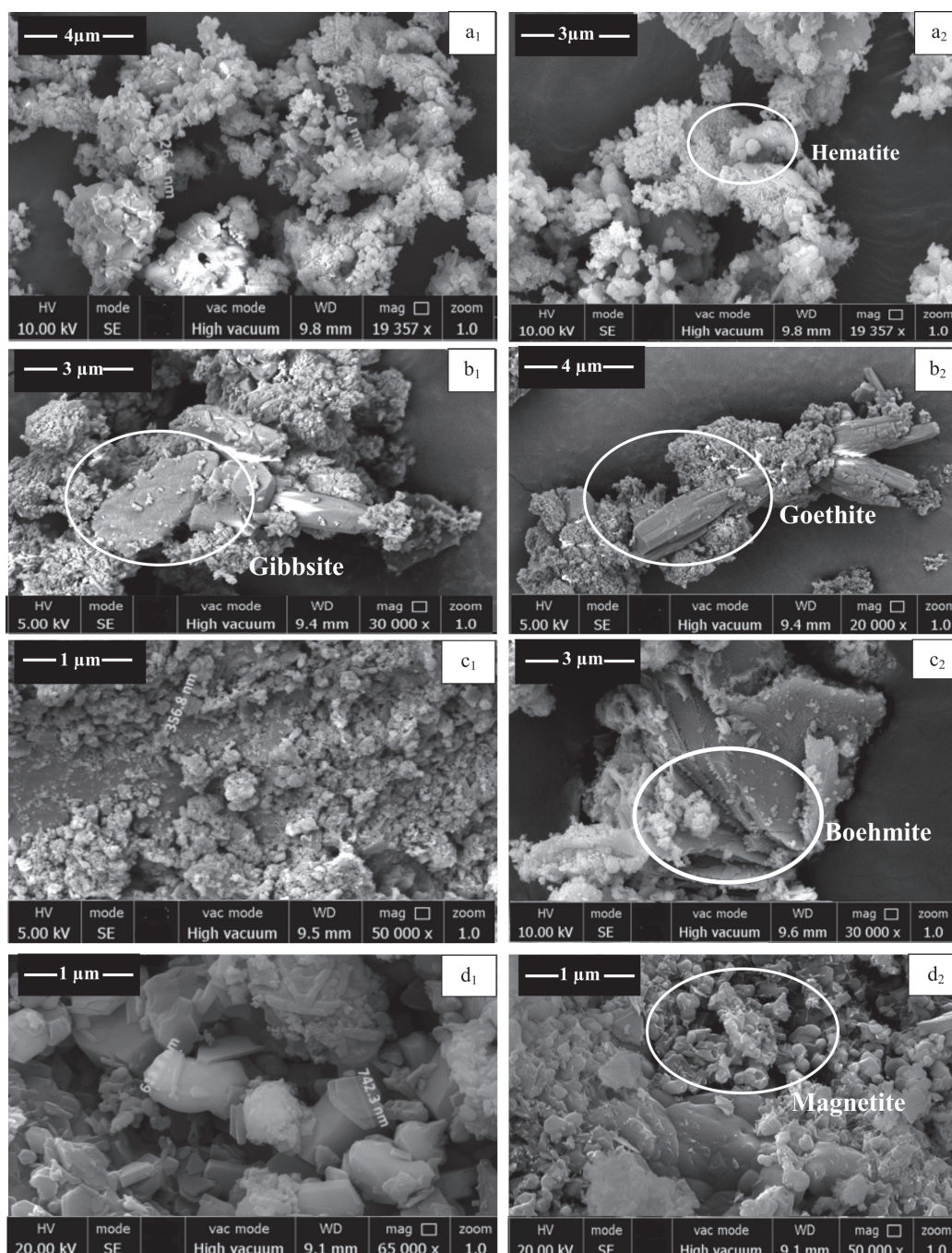


Fig. 5. FESEM images of a₁), a₂) Raw red mud b₁), b₂) RM650 c₁), c₂) RM 700 d₁), d₂) RM750.

with large particle size is obtained. The formation and rearrangement of the chemical composition of compounds result in a change in particle size and crystallinity improvement at higher calcination temperatures [29, 30]. The microstructure of raw red mud is comparatively unconfined, and the particle size is in the range of 800-1300 nm (Fig. 5a₁). Hematite is a spherical structure in raw red mud (Fig. 5a₂). The formation of intermediate compounds of magnetite at 650 and 700°C produce smaller particles ranging between 300-600 nm (Fig. 5c₁). The gibbsite was detected as a hexagonal plate-like structure at this stage, as in Figure 5b₁. At 750°C, the particle size has increased to 750-800 nm due to the gathering and formation of major compounds like magnetite (Fig. 5d₁).

The EDS (Fig. 6) shows the existence of oxides of Fe, Al, Si, Ca, and traces of Ti at different percentages. Fe present in small granular form is distributed uniformly, whereas flat and flaky particles represented as Al.

Calcination of red mud leads to the formation of intermediate compound $[\text{Fe}(\text{OH})_2(\text{OH})_4]^0$ due to the hydroxylation of ferrous ions. A further increase in temperature during the calcination process (at $\text{pH} > 7$) supports $\text{Fe}(\text{OH})_2$ precipitation and the product is sensitive to oxidation. Therefore, further increase in temperature forms various compounds such as goethite, magnetite and $\gamma\text{-FeOOH}$ precipitation, and the product is sensitive to oxidation. Therefore, further increase in temperature forms various compounds such as goethite, magnetite and $\gamma\text{-FeOOH}$, which is in the shape of lath (Fig. 5b₂, Fig. 5d₂, Fig. 6a) [29]. The

highly unstable intermediate compound with a poor structural organization, called ferrihydrite, is formed at the beginning of the calcination, which ultimately transforms into hematite particles. Therefore, at 750°C, these intermediate compounds' dehydration and local rearrangements lead to the production of magnetite, which has a globular shape (Fig. 5d₂). At the same time, gibbsite or bayerite (Fig. 7b, Fig. 7c) [31] and $\gamma\text{-AlOOH}$ boehmite (Fig. 7d) [32] were formed by aluminium in red mud under the same conditions.

Pozzolanic Activity

The compressive strength and strength activity index of the mortar mix after 7- and 28-days of curing in saturated $\text{Ca}(\text{OH})_2$ solution are illustrated in Fig. 8a) and Fig. 8b). As the cement is replaced by red mud, its compressive strength decreases.

Cement replaced with oven dried red mud (P1) showed the maximum decrement in the 7- and 28-day strength. However, cement replaced with RM700 (P3) gives comparable strength to the control mix and gives the highest SAI value to all other mixes. The mortar with the combination of cement and RM650 (P2) and cement and RM750 (P4) showed moderate SAI, respectively. P1, P2, P3, and P4 show 51, 11.5, 5.04, and 35.77% decrease in 28 days compressive strength compared to the control mix.

The strength activity index (SAI) graph is given in Fig. 8b). P3 and the lowest by P1 provide the highest SAI value. Strength activity is comparable for red mud

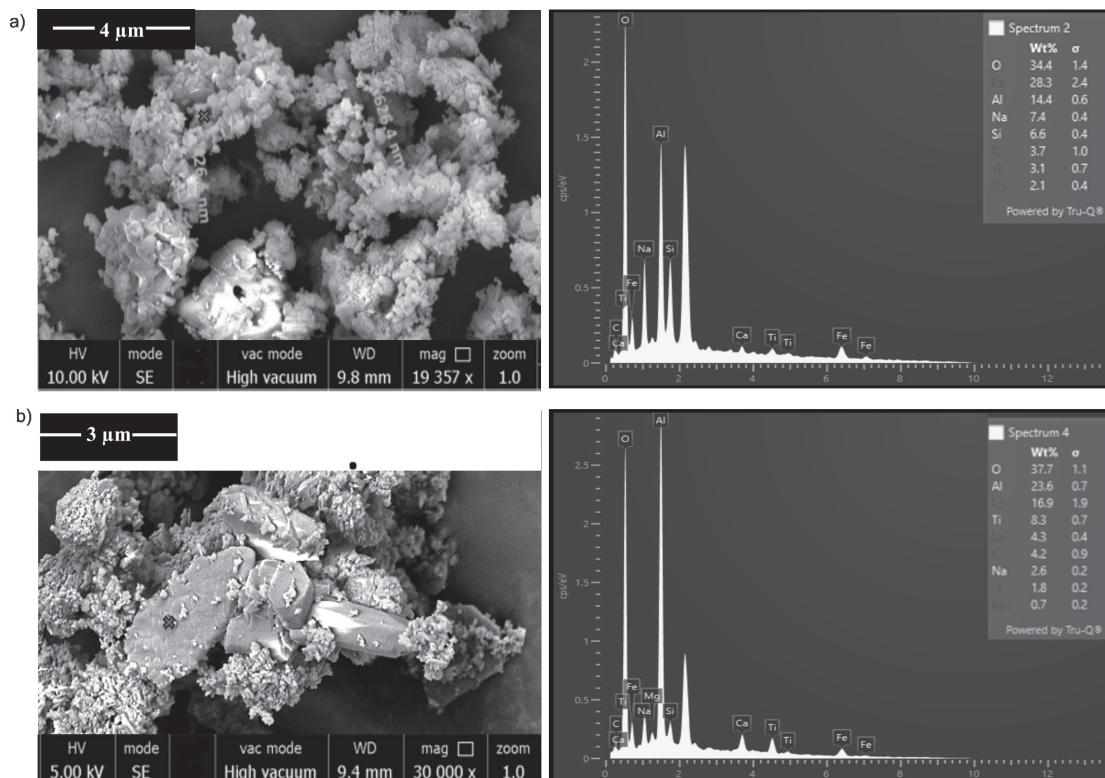


Fig. 6. a) Globular hematite b) Hexagonal gibbsite.

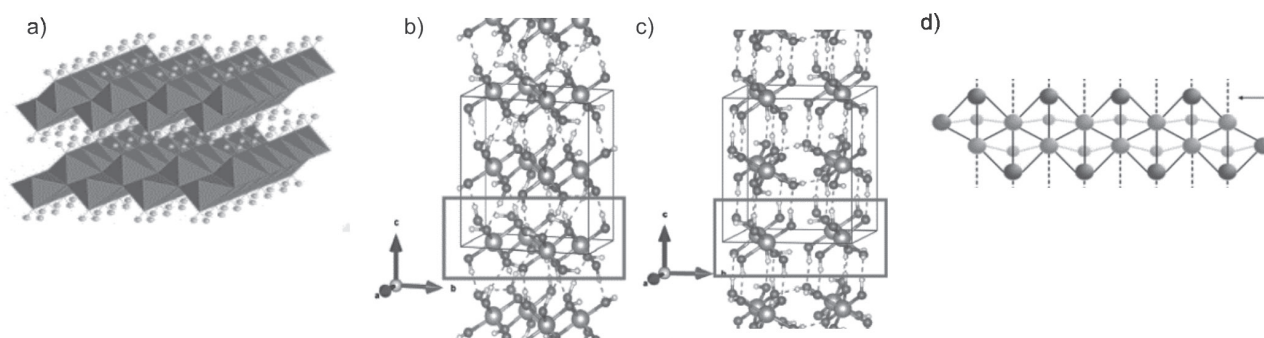


Fig. 7. Crystallised structure of a) γ -FeOOH b) gibbsite c) bayerite d) γ -AlOOH boehmite ([29, 32]).

samples calcined at 650 and 700°C for 7- and 28- day curing. RM750 reduces activity compared to red mud calcined at lower temperatures. It may be because, at higher calcination temperatures, the decarbonation of calcite to quick lime occurs, as explained in TGA [22]. Quick lime is less reactive than calcite to form other binding products in cement-based composites. Almost similar strength activity was observed for red mud

calcined at 650 and 700°C and cured for 7- and 28-day curing. However, a drastic decrease in strength activity was observed for red mud calcined at 750°C.

Also, the variation in SAI can be ascribed to the particle size distribution of raw and calcined red mud, that the size of the particles influences the pozzolanic activity of red mud. As the red mud became finer, the pozzolanic activity enhanced.

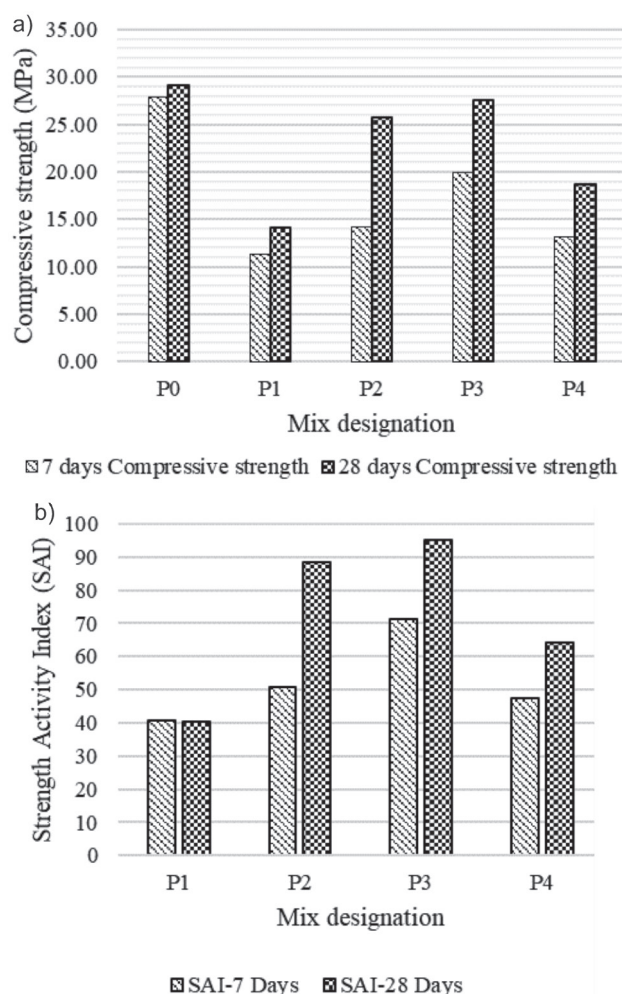
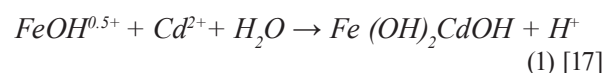


Fig. 8. a) 7and 28-day compressive strength for pozzolanic activity test b) Comparison of particle size and Strength activity index of red mud calcined at different temperature.

Metal Extraction

Fig. 9 shows the metal extraction efficiency of raw and calcined red mud obtained from atomic absorption spectroscopy (AAS). The concentration of Cd in standard solution is reduced by 0.85, 1.59, 1.19, and 1.26% by weight over time by raw red mud and red mud calcined at 650, 700, and 750°C respectively. The maximum metal extraction property was exhibited by red mud calcined at 650°C, and the minimum was by raw red mud. The formation of goethite at 650°C enhanced the Cd (II) extraction rate Eqn. [1] [17]. At 700°C, extraction is lesser than those at the other two calcination temperatures since the transition compounds present at 700°C are comparatively lesser reactive. The Cd (II) adsorbed spectrum of red mud shows a change in the crystallinity of silicate from 110 to 011. In the red mud calcined at 750°C after extraction, the alumina phase shifts from Al_2O_3 to $\sigma-Al_2O_3$ [17].



Cu extraction capacity of red mud samples is in the order of $RM650 \geq RM750 \geq RM700 \geq$ raw red mud. In raw red mud, boehmite is dominant compared to other calcined red mud. The calcination process improved the $CaCO_3$ content in red mud. Copper has more affinity to $CaCO_3$ than boehmite [33, 34]. Therefore, raw red mud shows the minimum capacity for Cu extraction. At the same time, calcined red mud has a better percentage of Cu extraction resulting in atomic absorption spectra (Eqn. [2]). Overall, more tight retention of Cu is possible in calcined red mud ($CaCO_3$ dominated) compared to raw red mud (boehmite dominated).

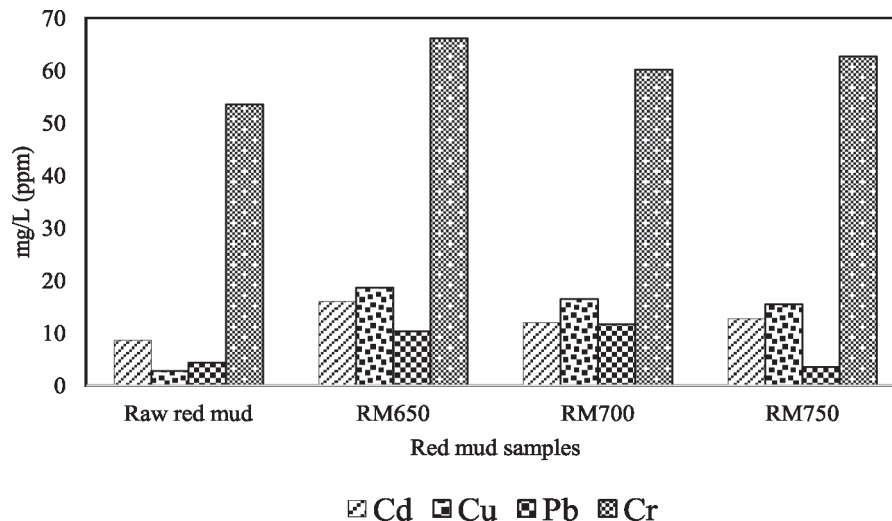
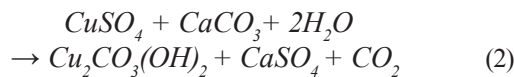


Fig. 9. Metal extraction results.



Pb (II) extraction mechanism reveals a strong affinity of Pb (II) ions to CaCO_3 . Ion exchange and precipitation combinedly contributed to the extraction of Pb. CaCO_3 interacted with Pb (II) in the solution to form $\text{Pb}(\text{CO}_3)_2(\text{OH})_2$ and PbCO_3 [35].

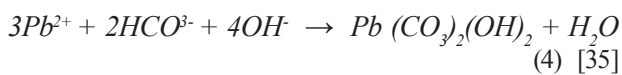
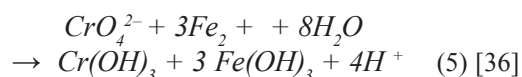


Fig. 9 shows that red mud is more efficient in extracting Cr (III) than other heavy metal ions. The mechanism explains that $\text{Cr}(\text{OH})_3$ is precipitated with red mud during the Cr (III) extraction. Fe (II) ions are oxidized in red mud at higher temperatures than Fe (III) ions. Fe (III) ion is highly efficient when reacting with Cr (III) and precipitates $\text{Cr}(\text{OH})_3$ and co-precipitate aluminium hydroxide. However, at a pH of >5 , Fe (II) is highly reactive to Cr (III) precipitation. Raw red mud is rich in Fe (II) with $\text{pH} > 5$, which is highly favourable for Cr (III) extraction. Also, RM650, RM700, and RM750 have Fe (III) ions with lower pH than raw red mud, which enhances the extraction process. Therefore, all samples show similar values on the Cr (III) extraction spectrum in AAS [36].



Statistical Analysis

The predictive values are drawn from the metal extraction experimental results as input for the regression analysis. The linear regression model is

adopted to develop the mathematical relation between the concentration of metal ions and mean extraction.

Eq. (6) is built with all continuous parameters. The effect of the concentration of metal ions with time on the metal extraction of the red mud is compared with the obtained mathematical model. The coefficient of the mathematical model was found with the least square method. The significance of the parameter in the statistical model was found from P-value. In the final equation, the parameter is considered significant when $P \leq 0.5$ and omitted when $P \geq 0.5$ [37].

The multi-collinearity in the model is analysed by Variance Inflation Factor (VIF). The yield stress can be quantified from the equation while a better correlation exists.

$$\text{Response} = \sum_{i=0}^n \alpha_i x_i + \epsilon \quad (6)$$

Where, x_i – variables or parameters,
 α_i – coefficients of the parameters,
 α_0 – constant term,
 Response – Shear stress.

Equation (7) and (8) give the regression equation for shear stress vs viscosity and shear stress vs torque.

$$\text{Concentration (ppm) (Cu)} = -0.068 + 14540 \text{ Mean extraction} \quad (7)$$

$$\text{Concentration (ppm) (Cr)} = -41.251 + 8326 \text{ Mean Extraction} \quad (8)$$

$$\text{Concentration (ppm) (Cd)} = -0.068 + 14540 \text{ Mean extraction} \quad (9)$$

$$\text{Concentration (ppm) (Pb)} = 0.323 + 6051 \text{ Mean Extraction} \quad (10)$$

Table 4. Model summary.

Sl no.	Parameters		Cu	Cr	Cd	Pb
1	Concentration (ppm)	F	238.11	398.97	238.11	502.15
		P	0.004	0.002	0.004	0.002
		VIF	1.00	1.00	1.00	1.00
2	S		0.34	0.46	0.34	0.32
3	R ²		99.17%	99.50	99.17%	99.60%
4	R ² (adjusted)		98.75%	99.25	98.75%	99.40%
5	R ² (predicted)		98.05%	97.41	98.05%	98.47%

The ANOVA is performed to analyze the statistical validity of the linear regression model on the concentration and the correlation with mean extraction. F and p-values obtained in the regression model indicate the best fit of the regression equation. The model summary is given in Table 4. The R^2 value indicates both concentration of metal ions vs mean extraction. $R^2 > 99\%$ indicates the statistical significance of the model and can be used to prediction of the newly designed experiments with the same boundary conditions [38]. The best fit is obtained in this model with a lower P-value (0.004, 0.002, 0.004, 0.002) and higher F-value (238.11, 398.97, 238.11, 502.15) for Cu, Cr, Cd, and Pb (Table 4). The higher values obtained for R^2 and the negligible value for lack-of-fit imply that no non-significant terms are involved in the model.

Conclusions

Following are the conclusions based on the analytical and statistical study.

1. The calcination process improved the reactive compound that enhances the pozzolanic activity of red mud.
2. Compared to raw red mud, RM750 has a larger particle size, and RM700 has the minimum particle size. The fineness of the particles increases the filling capacity of the red mud particles in the micropores and improves the pozzolanic activity.
3. Calcination enhanced the metal extraction property of red mud significantly. The metal extraction efficiency is in the order of Cr>Cd>Pb>Cu for each red mud sample. RM650 and RM700 show the maximum metal extraction efficiency compared to raw red mud.
4. Highest strength activity index (SAI), 7 and 28-day compressive strength were obtained for the mix with cement replaced by RM700 (P3) in the pozzolanic activity test.
5. The R^2 value of the regression models is greater than 99%. Hence the model is valid for any metal extraction experiments within the same boundary conditions. ANOVA analysis validates the regression model is statistically significant.

Acknowledgment

The authors gratefully acknowledge the testing labs of Vellore Institute of Technology, Vellore, for supplying facilities to carry out this research work.

Conflict of Interest

The authors declare no conflict of interest.

Reference

1. QURESHI H.J., AHMAD J., MAJDI A., SALEEM M.U., AL FUHAID A.F., ARIFUZZAMAN M. A Study on Sustainable Concrete with Partial Substitution of Cement with Red Mud: A Review. *Materials*, **15** (21), 7761, **2022**.
2. ZHAO S., MUHAMMAD F., YU L., XIA M., HUANG X., JIAO B., LI D. Solidification/stabilization of municipal solid waste incineration fly ash using uncalcined coal gangue-based alkali-activated cementitious materials. *Environmental Science and Pollution Research*, **26** (25), 25609, **2019**.
3. KOSHY N., DONDROB K., HU L., WEN Q., MEEGODA J.N. Synthesis and characterization of geopolymers derived from coal gangue, fly ash and red mud. *Construction and Building Materials*, **206**, 287, **2019**.
4. ANTUNES M.L.P., CONCEIÇÃO F.T., NAVARRO G.R.B., FERNANDES A.M., DURRANT S.F. Use of red mud activated at different temperatures as a low cost adsorbent of reactive dye. *Engenharia Sanitaria e Ambiental*, **26** (5), 805, **2021**.
5. KAYA K., SOYER-UZUN S. Evolution of structural characteristics and compressive strength in red mud-metakaolin based geopolymer systems. *Ceramics International*, **42** (6), 7406, **2016**.
6. CHEN H., WANG G., XU Y., CHEN Z., YIN F. Green process for supercritical water oxidation of sewage sludge with red mud as CO₂ absorbent. *Journal of Environmental Chemical Engineering*, **4** (3), 3065, **2016**.
7. NIKBIN I.M., ALIAGHAZADEH M., SH CHARKHTAB FATHOLLAHPOUR A. Environmental impacts and mechanical properties of lightweight concrete containing bauxite residue (red mud). *Journal of Cleaner Production*, **172**, 2683, **2016**.
8. AL-ZBOON K., AL-HARAHSEH M.S., HANI F.B. Fly ash-based geopolymer for Pb removal from aqueous

- solution. *Journal of Hazardous Materials*, **188** (1-3), 414, **2011**.
9. MOREIRA M.A.N.S., HEITMANN A.P., BEZERRA A.C.S., PATRÍCIO P.S.O., DE OLIVEIRA L.C.A., CASTRO C.S., DE SOUZA P.P. Photocatalytic performance of cementitious materials with addition of red mud and Nb₂O₅ particles. *Construction and Building Materials*, **259**, 119851, **2020**.
 10. PIETRELLI L., IPPOLITO N.M., FERRO S., DOVÌ V.G., VOCCIANTE M. Removal of Mn and As from drinking water by red mud and pyrolusite. *Journal of Environmental Management*, **237**, 526, **2019**.
 11. SHI W., REN H., HUANG X., LI M., TANG Y., GUO F. Low cost red mud modified graphitic carbon nitride for the removal of organic pollutants in wastewater by the synergistic effect of adsorption and photocatalysis. *Separation and Purification Technology*, **237** (October 2019), 116477, **2020**.
 12. SHI W., REN H., LI M., SHU K., XU Y., YAN C., TANG Y. Tetracycline removal from aqueous solution by visible-light-driven photocatalytic degradation with low cost red mud wastes. *Chemical Engineering Journal*, **382** (June 2019), 122876, **2020**.
 13. OPRČKAL P., MLADENVIČ A., ZUPANČIČ N., ŠČANČAR J., MILAČIČ R., ZALAR SERJUN V. Remediation of contaminated soil by red mud and paper ash. *Journal of Cleaner Production*, **256**, **2020**.
 14. CHEN X., GUO Y., DING S., ZHANG H., XIA F., WANG J., ZHOU M. Utilization of red mud in geopolymer-based pervious concrete with function of adsorption of heavy metal ions. *Journal of Cleaner Production*, **207**, 789, **2019**.
 15. KARUNADASA K.S.P., MANORATNE C.H., PITAWALA H.M.T.G.A., RAJAPAKSE R.M.G. Thermal decomposition of calcium carbonate (calcite polymorph) as examined by in-situ high-temperature X-ray powder diffraction. *Journal of Physics and Chemistry of Solids*, **134** (January), 21, **2019**.
 16. ASTM C 311-22. Standard Test Methods for Sampling and Testing Fly Ash or Natural Pozzolans for Use in Portland-Cement Concrete. *Annual Book of ASTM Standards*, 04.02, 1, **2022**.
 17. RAO K., MOHAPATRA M., ANAND S., VENKATESWARLU P. Review on cadmium removal from aqueous solutions. *International Journal of Engineering, Science and Technology*, **2** (7), 81, **2011**.
 18. ZINOVEEV D., PASECHNIK L., FEDOTOV M., DYUBANOV V., GRUDINSKY P., ALPATOV A. Extraction of valuable elements from red mud with a focus on using liquid media – a review. *Recycling*, **6** (2), **2021**.
 19. TSAMO C., DJOMOU DJONGA P.N., DANGWANG DIKDIM J.M., KAMGA R. Kinetic and Equilibrium Studies of Cr(VI), Cu(II) and Pb(II) Removal from Aqueous Solution Using Red Mud, a Low-Cost Adsorbent. *Arabian Journal for Science and Engineering*, **43** (5), 2353, **2018**.
 20. WU C.S., LIU D.Y. Mineral phase and physical properties of red mud calcined at different temperatures. *Journal of Nanomaterials*, **2012** (3), **2012**.
 21. DODOO-ARHIN D., NUAMAH R.A., AGYEI-TUFFOUR B., OBADA D.O., YAYA A. Awaso bauxite red mud-cement based composites: Characterisation for pavement applications. *Case Studies in Construction Materials*, **7** (June), 45, **2017**.
 22. CASTALDI P., SILVETTI M., SANTONA L., ENZO S., MELIS P. XRD, FTIR, and thermal analysis of bauxite ore-processing waste (red mud) exchanged with heavy metals. *Clays and Clay Minerals*, **56** (4), 461, **2008**.
 23. ANTUNES M.L.P., COUPERTHWAITTE S.J., DA CONCEIÇÃO FT., DE JESUS C.P.C., KIYOHARA P.K., COELHO A.C.V., FROST R.L. Red mud from Brazil: Thermal behavior and physical properties. *Industrial and Engineering Chemistry Research*, **51** (2), 775, **2012**.
 24. J. PERA, R. BOUMAZA, J.A. Development of a pozzolanic pigment from red mud. *Journal of Cement and Concrete Research*, **27** (10), 1513, **1997**.
 25. MANFROI E.P., CHERIAF M., ROCHA J.C. Microstructure, mineralogy and environmental evaluation of cementitious composites produced with red mud waste. *Construction and Building Materials*, **67**, 29, **2014**.
 26. ALELWEET O., PAVIA S., LEI Z. Pozzolanic and Cementing Activity of Raw and Pyro-Processed Saudi Arabian Red Mud (RM) Waste. *Recent Progress in Materials*, **3** (4), 1, **2021**.
 27. LU Y., LIU X., YU L., ZHANG X., DUAN W., PARK J., DONG X. Removal Characteristics and Mechanism of Mn(II) from Acidic Wastewater Using Red Mud-Loess Mixture. *Polish Journal of Environmental Studies*, **31** (6), 5781, **2022**.
 28. BORRAJO J.P., LISTE S., SERRA J., GONZÁLEZ P., CHIUSI S., LEÓN B., HUPA M. Influence of the Network Modifier Content on the Bioactivity of Silicate Glasses. *Key Engineering Materials*, **254-256** (January), 23, **2004**.
 29. JOLIVET J.P., TRONC E., CHANÉAC C. Iron oxides: From molecular clusters to solid. A nice example of chemical versatility. *Comptes Rendus - Geoscience*, **338** (6-7), 488, **2006**.
 30. SOO J.Z., ANG B.C., ONG B.H. Influence of calcination on the morphology and crystallinity of titanium dioxide nanofibers towards enhancing photocatalytic dye degradation. *Materials Research Express*, **6** (2), **2019**.
 31. KIM D., JUNG J.H., IHM J. Theoretical study of aluminum hydroxide as a hydrogen-bonded layered material. *Nanomaterials*, **8** (6), 1, **2018**.
 32. CHOI E.G., SONG K.H., AN S.R., LEE K.Y., YOUN M.H., PARK K.T., KIM H.J. Cu/ZnO/AlOOH catalyst for methanol synthesis through CO₂ hydrogenation. *Korean Journal of Chemical Engineering*, **35** (1), 73, **2018**.
 33. MA Y., SI C., LIN C. Comparison of copper scavenging capacity between two different red mud types. *Materials*, **5** (9), 1708, **2012**.
 34. RICHARD K. *Red Mud: Production, Composition and Impact*. Nova Science Publishers Inc. **2018**.
 35. LYU F., NIU S., WANG L., LIU R., SUN W., HE D. Efficient removal of Pb (II) ions from aqueous solution by modified red mud. *Journal of Hazardous Materials*, **406** (September 2020), 124678, **2021**.
 36. SHARMA S.K., PETRUSEVSKI B., AMY G. Review Paper Chromium removal from water: a review. **2008**.
 37. DAHASAHA STRA A.V., BALASUNDARAM K., LATKAR M. V. Hydrometallurgy Turbidity removal from synthetic turbid water using coagulant recovered from water treatment sludge : A potential method to recycle and conserve aluminium. *Hydrometallurgy*, **213**, 105939, **2022**.
 38. MONTGOMERY D.C. *Design and Analysis of Experiments*. Mycological Research (9th Editio., Vol. **106**). Wiley. **2017**.